

Article

Prediction of Tunnelling Parameters for Underwater Shield Tunnels, Based on the GA-BPNN Method

Yu Liang ^{1,2,*} , Kai Jiang ¹, Shijun Gao ³ and Yihao Yin ³

¹ School of Civil Engineering, Shenzhen Campus of Sun Yat-sen University, Shenzhen 518000, China

² School of Civil Engineering, Sun Yat-sen University, Zhuhai 519000, China

³ China Railway 14th Bureau Group Mega Shield Construction Engineering Co., Ltd., Nanjing 210000, China

* Correspondence: liangyu25@mail.sysu.edu.cn

Abstract: Reasonable tunnelling parameters for underwater shield tunnels play an important role in maintaining driving efficiency and safety. In this paper, a neural network method was developed to predict tunnelling parameters. Soil properties and geometric parameters were taken as inputs for the neural network, which output the tunnelling parameters, such as advancing thrust, rotation, penetration, torque of the cutter head, and support pressure. In order to improve the stability of the neural network, a genetic algorithm (GA) with a global searching ability was used to optimize the initial weight of the neural network (GA-BPNN). The accuracy of the algorithm, based on GA-BPNN, was studied through an underwater shield tunnel project. The results showed that the integration of GA into the neural network significantly improves the prediction ability for shield tunnelling parameters, especially for adjustable parameters. Later, the developed GA-BPNN model was further utilized to predict and set the range of shield tunnelling parameters in fine sand stratum of high risk. Through a comparative analysis of tunnelling parameters, the reasons leading to ground instability have been found out, and the effectiveness of ground pre-reinforcement has been verified.

Keywords: genetic algorithm; back propagation neural networks; shield tunneling; operational parameters prediction; ground reinforcement evaluation



Citation: Liang, Y.; Jiang, K.; Gao, S.; Yin, Y. Prediction of Tunnelling Parameters for Underwater Shield Tunnels, Based on the GA-BPNN Method. *Sustainability* **2022**, *14*, 13420. <https://doi.org/10.3390/su142013420>

Academic Editor: Syed Minhaj Saleem Kazmi

Received: 15 September 2022

Accepted: 12 October 2022

Published: 18 October 2022

Publisher's Note: MDPI stays neutral with regard to jurisdictional claims in published maps and institutional affiliations.



Copyright: © 2022 by the authors. Licensee MDPI, Basel, Switzerland. This article is an open access article distributed under the terms and conditions of the Creative Commons Attribution (CC BY) license (<https://creativecommons.org/licenses/by/4.0/>).

1. Introduction

Underwater shield tunnels have been widely constructed for underwater transportation in China, since 2003. As of June 2022, at least 80 large-diameter shield tunnels (diameters greater than 10 m) have been constructed or are under construction, among which more than 46 tunnels are characterized as having diameters greater than 14 m, as shown in Figure 1.

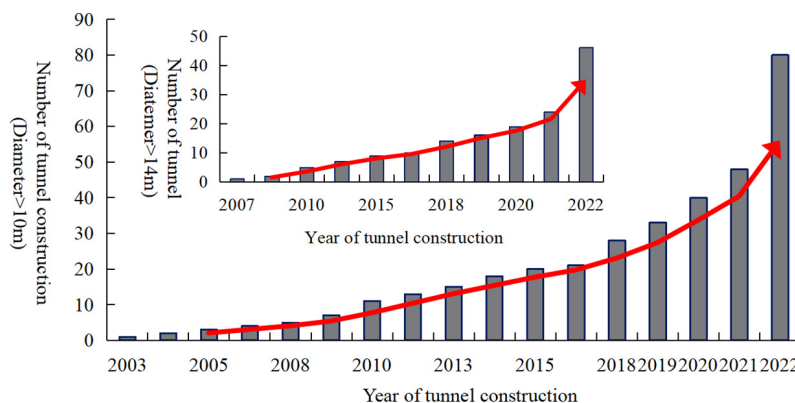


Figure 1. Survey of large-diameter underwater shield tunnel construction in China.

Compared with common shield tunnelling, shield tunnelling across rivers or seas is more complex. Typical challenges for underwater tunnelling include shallow overburden, high water pressure, and geological uncertainty, which result in the instability of the excavation face, inadequate performance of the excavation, schedule delay, and cost overrun [1]. Knowing how to ascertain and control the operation of underwater shield tunnelling processes is of the utmost importance [2].

As it is known, the operational parameters for shield tunnelling include the rotational speed of the cutter head, advancing thrust, working pressure (support pressure), penetration rate, torque, and advance speed [3]. Among these parameters, the rotational speed of the cutter head, advancing thrust, and working pressure are the three main operational parameters that can be directly adjusted in a slurry shield machine. The rest of the parameters vary according to changes in the three main adjustable parameters. For example, with the same rotational speed, an increase in thrust would lead to an increase in torque, which would further result in a greater penetration rate and would enhance the tunnelling speed. However, the rise of both the penetration rate and the tunnelling speed may result in significant ground deformation or instability on the excavation face, without careful control in tunnelling. This is mainly owing to the fact that the tunnelling parameters are highly nonlinear, particularly in cases with stratigraphic uncertainty, soil heterogeneity, various loading conditions, and complex TBM–soil interaction [4]. Therefore, how to adopt appropriate shield tunnelling parameters to match the state of the given soil/rock stratum, is the premise of realizing intelligent control of shield tunnel machines.

Over the years, a number of investigations have been conducted to determine the optimum operational parameters during shield tunnelling, and these approaches can be generally classified into the following four types: numerical simulation, physical experiment, analytical models, and statistical models [5]. Among numerous analytical approaches, perhaps the deterministic model is the most commonly used, owing to its simplicity in formulation and high efficiency in computation. The most recognized deterministic model, the CSM model (including the improved CSM model), was developed by the Colorado School of Mines [6,7]. In CSM, the relationships among the operational parameters are established based on rock fragmentation mechanisms. As an alternative, a model based on optimum energy has been proposed to select TBM tunnelling parameters in hard rock. The relationships among energy, geological conditions, and the TBM construction performance are analyzed by combining the results from the LCM tests and the on-site data [8]. However, due to a lack of sufficient input data, the accuracy of this approach seems relatively low. In addition, the uncertainties of the predictive tunnelling parameters are ignored by the deterministic model [1], thus limiting its application.

The statistical approach is based on field monitoring data, with the application of regression methods, thus, the responses of shield tunnelling parameters upon their influencing factors can be characterized. Typical examples in this approach include NTNU [9], QTBM [10], RME [11], FPI [12,13], RMR [14], and GSI [15]. Stochastic theory has also been adopted in the statistical model for the estimation of the penetration rate, advance rate, thrust and torque requirements, and for assessing the probability of uncertainties/risks and predicting the varying shield operation parameters [5]. Recently, the visibility graph model has been employed to study the correlations among the tunnelling operational parameters under both static and dynamic conditions [4]. The statistical analysis is pragmatic for the understanding of shield tunnelling performance.

As it is known, the shield tunnelling parameters are mainly influenced by factors such as the tunnel depth, water table, geological conditions, and the strength of soil/rock mass [16]. The relationships among the tunnelling parameters and their influencing factors can be characterized by a high-order, nonlinear fuzzy system, which is difficult to express through an explicit function. To tackle this problem, the artificial intelligence method has been applied by many scholars to estimate the performance of shield tunnelling. This is mainly owing to the fact that the artificial intelligence method is featured with strong parallel processing capability and nonlinear approximation characteristics, which ignore

the mechanical calculation process and avoid the impacts induced by various construction factors. For example, the effectiveness of the prediction model, based on the support vector regression (SVR) algorithm, can be evaluated through statistical indicators, with high correlations among the predicted and measured parameters being achieved [16,17]. Other approaches, such as particle swarm optimization (PSO), differential evolution (DE), grey wolf optimizer (GWO) [18], and the fuzzy logic [19] method, have been employed to predict the shield penetration rate, with acceptable results. The data-driven technique (DDT), recurrent neural networks (RNNs), long-short term memory (LSTM), gated recurrent unit (GRU), and the cluster analysis (CA) method have also been adopted to predict the shield tunnelling parameters [20–22]. These studies reflect the rapid development of artificial intelligence in the understanding of nonlinear relationships among the tunnelling parameters and their influencing factors. Note that the back propagation neural network (BPNN), trained by the gradient descent method, is one of the most promising artificial intelligence methods [23]. However, the model is very sensitive to the initial network weight, and, when the network is initialized with different weights, the model may converge to different local minima, which affects the performance of the overall optimization procedure in this algorithm. To overcome this shortcoming, hybrid intelligence optimization methods are adopted and integrated into the neural network [14,24]. The genetic algorithm (GA) is a heuristic global random search method, which can effectively avoid the parameter optimization in local converge. The hybrid GA-BPNN has been applied in some engineering fields, such as for automotive suspension systems, phased array radars, and aircraft scheduling problems. [25,26].

Numerous studies have been carried out on shield tunnelling parameters, which have also advanced the operational technology for shield tunnelling. However, most of the aforementioned studies have focused on hard rock mass, and studies on shield tunnelling in composite formation or underwater have been very limited. To achieve this in the current study, software was developed using programming language C# and Matlab. Based on an underwater shield tunnel project in China, the predicted tunnelling parameters obtained from both traditional BPNN and GA-BPNN were compared with the field operational data. Later, the developed GA-BPNN model was further utilized to predict the shield operational parameters in fine sand stratum of high risk. Based on the parameter analysis, the driving reasons that lead to ground instability have been found out, and the effectiveness of ground pre-reinforcement has been verified. This case study demonstrates the applicability of GA-BPNN for underwater shield tunnelling, and deep discussions are presented.

2. Methodology

Artificial Neural Network and GA-BPNN

Artificial neural networks (ANN) originated in the 1940s. It is a complex network system that consists of a large number of interconnected simple processing units (neurons). It reflects many basic features of the human brain and is a highly complex, nonlinear dynamic system. ANN is characterized by large-scale parallelism, distributed storage and processing, self-organization, self-adaptation, and self-learning. It is suitable for fuzzy problems, with the ability to consider multiple factors at the same time, thus reflecting the causality hidden in a variety of samples. The ANN models can be classified into a few classes, such as feedforward type, feedback type, self-organizing type, and random type [27].

Back propagation neural network (BPNN) is a type of feedforward neural network, with strong self-learning ability. The weights of BPNN are adjusted by back propagation learning algorithm. However, the neural network, trained by back propagation algorithm (i.e., the gradient descent algorithm), often takes a long time to converge. In addition, it inevitably encounters the local optimal problem, thus failing to find the global optimal solution [28].

Genetic algorithm (GA) is an optimization algorithm that originated from the theory of biology evolution. It provides a new way to solve problems that traditional optimization

methods struggle to solve. GA generally includes the following four operation components: population initialization, selection, crossover, and mutation. The search and optimization of GA is not dependent on the gradient information. Though the defined fitness function is discontinuous and irregular, the global optimal solution still can be found with great probability. Therefore, GA can be suitable for the weight optimization of BPNN. The improved hybrid method is called GA-BPNN. The main steps of GA to optimize BPNN connection weight are as follows:

- (1) Determine the structure of BP neural network and set various parameters, such as initial weight and threshold.
- (2) Initialize the population of GA, including initialization of population size, crossover probability, mutation probability, and weight.
- (3) The fitness value of each individual in the population is calculated.
- (4) Each individual is randomly selected for replication, crossover, and mutation, to produce new individuals with certain probability, which inherit the high-quality genes of individuals in the population to obtain new, excellent populations.
- (5) Calculate whether the number of iterations in the new population reaches the maximum genetic algebra and perform the judgment operation. If the results meet the qualification, the inheritance ends, if not, go back to step (3).
- (6) Calculate the fitness values in the population, output and decode the most adaptive individual to obtain the global optimal initial weight and threshold in the network model.
- (7) Input the initial weight and threshold adjusted by the genetic algorithm into the BP neural network, then the network training is performed to determine whether the experimental accuracy meets the required qualification.

During BP forward propagation process, the information is passed from the input layer to the hidden layer, and then to the output layer. The error between output and actual value is calculated and passed from the output layer to the hidden layer, and then to the input layer by back propagation. The weights are fixed and the objective function is minimized during this process. GA is used to search the optimal weight and reduce its initial error, which is then assigned to BP network. The algorithm flow chart is shown in Figure 2. After the initial set obtained by gradient descent of traditional BPNN, the GA is implemented to calculate more suitable weights.

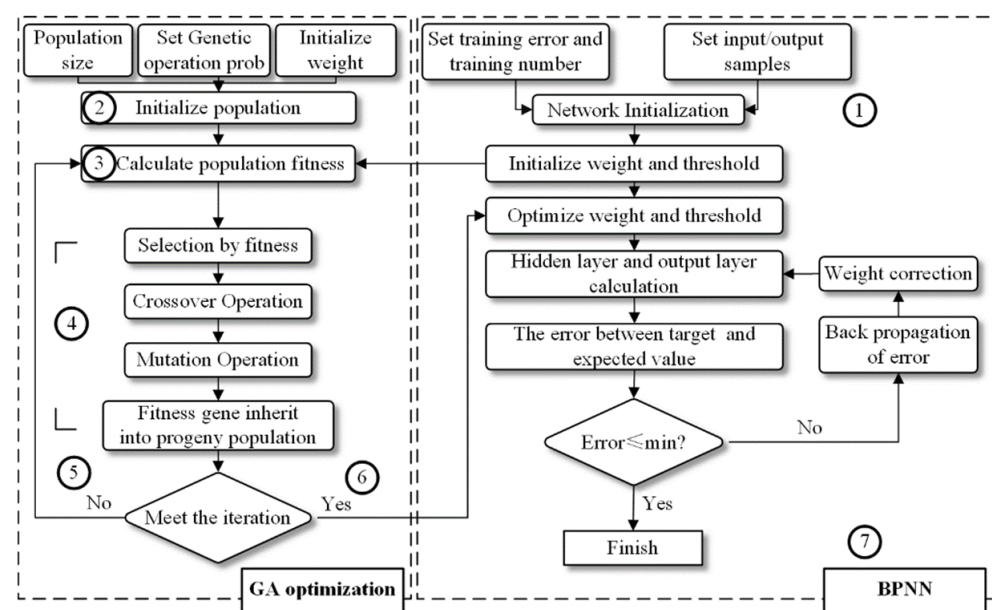


Figure 2. The flow chart of BPNN, optimized by GA (GA-BPNN).

3. Case Study: An Underwater Tunnel Project

3.1. The Underwater Tunnel Overview

The underwater tunnel project was launched to link the two banks, which are located in China. Two separate tunnels were included in this project: the northern tunnel (1615 m long, tunneled first) and the southern tunnel (1423 m long, tunneled after the northern tunnel was accomplished). The slurry shield started tunnelling from the east bank to the west bank. A ring of tunnel lining was assembled by nine segments. The outer diameter of the tunnel was 11.3 m, the thickness and width of the segments were 0.5 m and 2.0 m, respectively. The twin tunnels were mainly located in the weathered conglomerate stratum. The overlying soil was mainly sandy soil. When the shield first approached the west bank (the northern tunnel), a surface collapse accident occurred in front of the shield cutter (as shown in Figure 3). As the shield continued to advance, several small-scale collapses occurred successively.



Figure 3. Overview of the underwater tunnels.

It is considered that the ground surface collapse was caused by the mismatch between the tunnelling parameters and the formation condition. Apart from the failure of the shield machine and the operation factors, the shield tunnelling performance was mainly affected by geometry characteristics and the geological conditions. Geometry characteristics impose a significant impact on the settlements and excavation face stability of shield-driven tunnels. Typical parameters include the depth of the tunnel axis from the ground level, H , and the tunnel diameter, D . Soil properties, such as unit weight, cohesion, friction angle, load-bearing capacity, and permeability, are considered as geological factors. Undoubtedly, the stability of the shield tunnelling process depends on the interaction between the machine and the ground [2]. From the literature review, five factors, including the rotation, penetration, torque of the cutter head, advancing thrust, and the working chamber pressure (support pressure) are the most basic criteria for judging excavation efficiency, among the shield tunnelling parameters [29]. Other parameters, e.g., shield advance rate, utilization rate, energy consumption, and cutter life, are less important and are not discussed here.

To ensure the safety of the subsequent tunnelling (southern tunnel), the BPNN and GA-BPNN method were adopted to predict the tunnelling parameters, and the effectiveness of the above methods were verified. The corresponding parameters of the south line (tunnel segments number 50–549, 500 rings) were selected with BPNN and GA-BPNN. The parameters at segments number 50–499 were taken as the training data, and that of segments number 500–549 were taken as the prediction data (Figure 4).

Based on the information of every drilling hole from a detailed exploration, the soil properties at each section (numbered by tunnel segments) were obtained by the weighted average method. The average distance between adjacent drilling holes was approximately 30 m, they were located on the tunnel axis. The existing data were classified into the following two categories before the application of the artificial neural network: one class of input variables to reflect the external environment factors, and another class of output variables to reflect the shield tunnelling performance. The ratio of the cover depth to

the tunnel diameter (H/D), underground water level (H_w), weighted unit weight (γ_0), weighted cohesive (c), weighted internal friction (φ), weighted lateral pressure coefficient (K), weighted permeability coefficient (K_i), and weighted Poisson's ratio (μ) of the stratum were selected as the input data. The rotation (R), penetration (P), torque (T) of the cutter head, advancing thrust (F), and support pressure (W_p) of the shield were considered as output data. The physical and mechanical properties of each stratum above the tunnel are shown in Table 1.

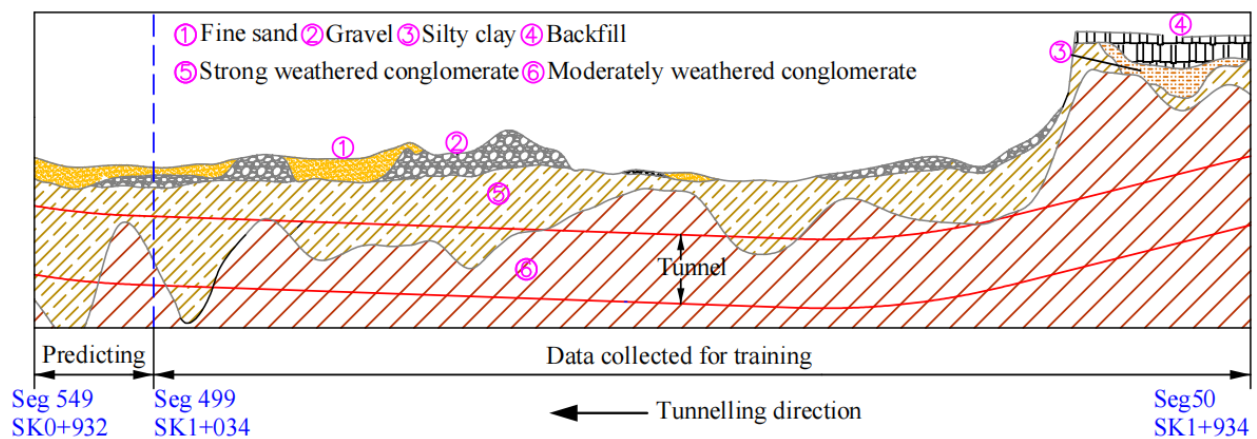


Figure 4. Samples collected for BPNN and GA-BPNN.

Table 1. Physical and mechanical properties of each stratum above tunnel.

Stratum	Natural Gravity (kN/m^3)	Cohesion (kPa)	Friction Angle ($^\circ$)	Poisson Ratio	Permeability Coefficient (m/d)	Lateral Pressure Coefficient
Fine sand	19.9	5	18	0.30	7.5	0.43
Gravel	21.0	0	35	0.28	17.8	0.39
Silty clay	19.2	40	18	0.32	0.02	0.30
Backfill	19.5	12	8	0.35	1.25	0.54
Conglomerate (strong weathered)	23.5	185	32	0.25	0.16	0.33
Conglomerate (moderate weathered)	24.3	500	38	0.22	0.11	0.28

3.2. Parameter Settings for BPNN and GA-BPNN

Proper parameter settings are of significant importance in the training process of ANN [30]. Two aspects are considered to affect the model's performance: the first one is the network structure, including the number of the input layer, hidden layer, and output layer; the second is the connection the weights among the adjacent nodes. The node number of the output layer and input layer are usually determined by the application requirement, however, that of the hidden layer relies on the experience of the user. Trial tests are usually taken to obtain the optimal number of hidden layer nodes. This process is continued until the optimal number of hidden layer nodes is obtained, thus approaching the highest accuracy. After a few trial tests, the number of nodes was set as 17 in this case. The learning rate refers to the iterative step length of the model, which is usually set between 0.01 and 0.9. The smaller the learning rate, the smaller the step length, and, thus, the more times are needed to train the model. The learning rate was set as 0.1 in this project. The TanSig and Purelin functions were adopted as the transfer functions in the hidden and output layers, respectively. The training times were set to 20,000, and the convergence rate was set to 0.01.

The optimization parameters of GA include the population size, iteration times, crossover probability, and the mutation probability. Among them, population size is a preset parameter, which represents the number of individuals, the size of which depends on the complexity of the problem. According to previous research [31], the population size can be taken from $4n$ to $6n$, where n is the number of the input variable. Another important parameter, crossover probability, is adopted to simulate the mating process in biological evolution. In this process, individuals exchange genes with a certain probability in an iterative process. The crossover probability should be set properly to avoid losing the optimal individuals or falling into the local optimal. The crossover probability of a given population is usually between 0.6 and 1.0. Mutation probability is another way to simulate the generation of new individuals, but it is more sensitive to the population. Generally, the mutation probability is set to be small, ranging from 0 to 0.2, based on a user's experience. The iterations of the population, according to relevant studies, are generally between 100 and 1000. Based on the uniform design method, dozens of the parameter combinations were tested in this case, until the optimal value was obtained, as shown in Table 2.

Table 2. Algorithm parameters for GA-BPNN.

Parameters for BPNN	Nodes in Hidden Layer	Learning Rate	Training Times	Convergence Rate
	17	0.1	20,000	0.01
Parameters for GA	Population Size	Crossover Probability	Mutation Probability	Population Iterations
	50	0.6	0.2	300

The traditional BPNN was used for training, with the training error curve being obtained (taking support pressure (W_p) as an example) as shown in Figure 5a. After 20,000 trainings, the training error decreased from 0.3924 to 0.0319. Although the error did not reach the set convergence rate (0.01), the network approached stable. The optimal weights obtained by GA were assigned to BPNN to establish a nonlinear relationship between the input data and the output data. The training error curve is shown in Figure 5b. After 20,000 trainings, the training error decreased from 0.0189 to 0.0085, indicating that the network was stable. This also indicated that the GA-BPNN performs better than traditional BPNN.

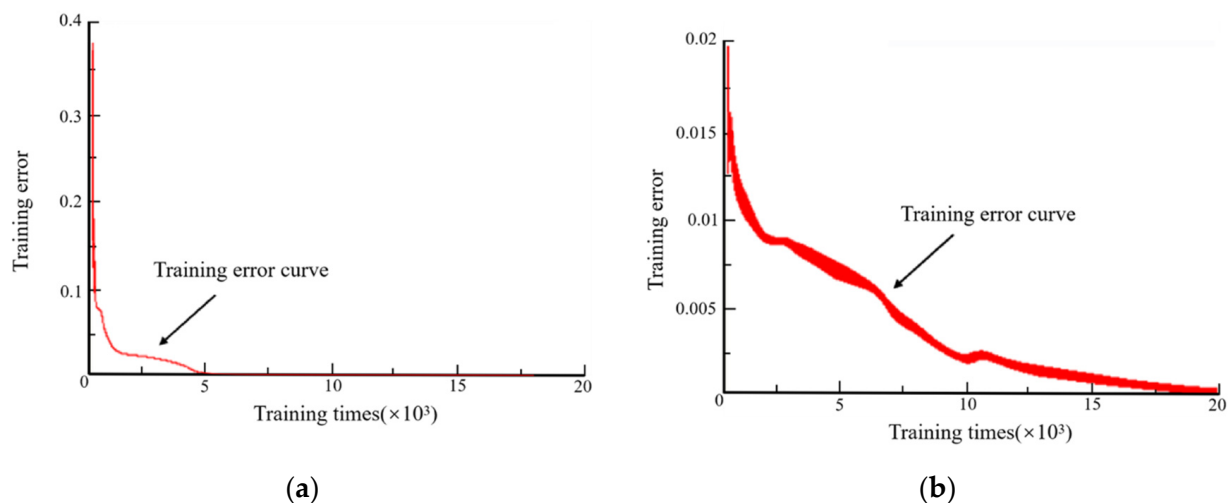


Figure 5. Network training results curve (support pressure): (a) training error curve of BPNN and (b) training error curve of GA-BPNN.

4. Results and Discussion

4.1. Prediction Result with BPNN

As mentioned above, 450 samples from the southern line (tunnel segments number 50–499), were selected as the training data. First, the data of 450 samples were trained with BPNN (not optimized by GA), after that, the trained model was adopted to predict the tunnelling parameters at the same interval, with which the measured tunnelling parameters were compared, as shown in Figure 6. The trained values were consistent with the measured values, with low divergences. The trained results of all the parameters were accurate and acceptable.

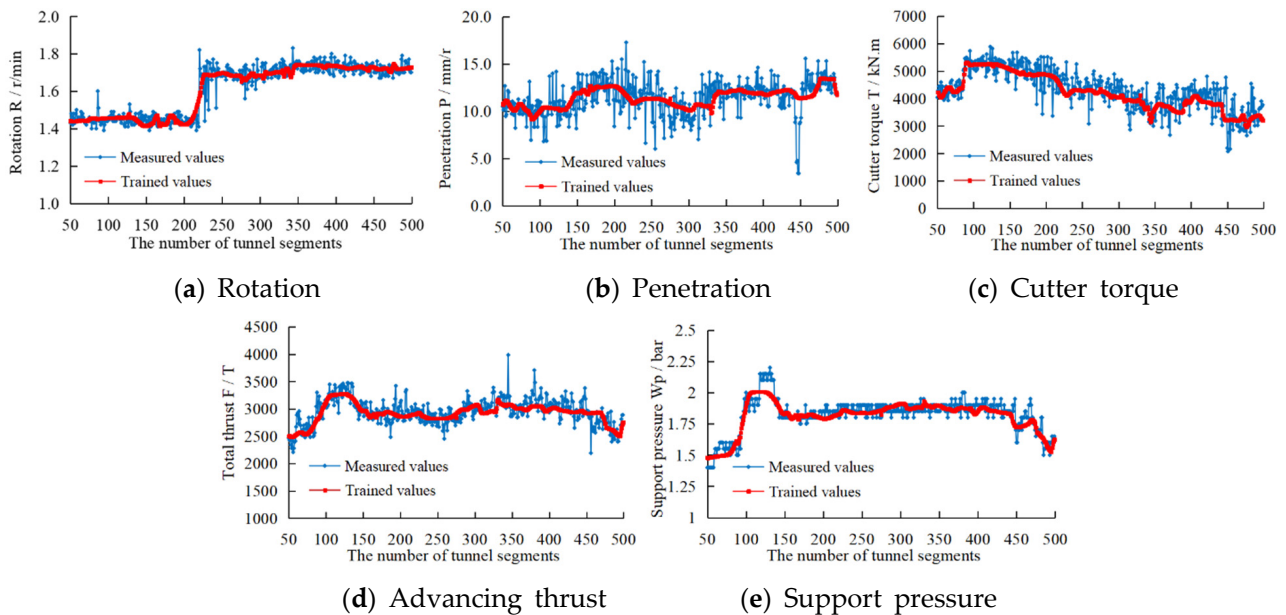


Figure 6. Trained and measured tunnelling parameters of BPNN: (a) rotation; (b) penetration; (c) cutter torque; (d) advancing thrust; and (e) support pressure.

To verify the prediction accuracy of the BPNN model, the trained model was applied to predict the subsequent tunnelling parameters of the southern tunnel (tunnel segments number 500–549, 50 samples, see Figure 4). The predicted and measured values are shown in Figure 7. The variation trend of the predicted values still showed a relatively good fit with the measured values, however, there may be local optimal problems in some intervals. For example, the predicted support pressure (W_p) failed to fit the measured values in the second half of the curve (segments number 520–549), as shown in the dotted circle in Figure 7. This could be explained by the local optimal problem in BPNN.

4.2. Prediction Result with GA-BPNN

The same parameters of the southern line (tunnel segments number 50–499, 450 samples) were selected as the training data, and trained with the GA-BPNN method, as shown in Figure 8. Compared with the BPNN model, the trained data obtained by the GA-BPNN model were closer to the measured results, with better fitting agreement.

To verify the generalization of the GA-BPNN model, the model was applied to the same intervals of the underwater tunnel (tunnel segments number 500–549, 50 samples). The predicted and measured values are shown in Figure 9. Compared with Figure 7, a more consistent trend between the predicted and measured parameters can be observed in Figure 9, and local optimal problems did not occur, demonstrating the capacity of the developed model (GA-BPNN).

To further quantify the model's accuracy, the mean absolute percentage error (MAPE) and the root mean square error (RMSE) were adopted to describe and compare the prediction effects of the two methods.

$$MAPE = \frac{1}{n} \sum_{i=1}^n \left| \frac{\hat{y}_i - y_i}{y_i} \right|, \quad (1)$$

$$RMSE = \sqrt{\frac{1}{n} \sum_{i=1}^n (\hat{y}_i - y_i)^2}, \quad (2)$$

where \hat{y}_i is the predicted value for a single sample, y_i is the expected value for a single sample. Note that different tunnelling parameters have different dimensions and units, which will affect the prediction accuracy. In this paper, the min.–max. normalization method was adopted to solve the dimensional effects among the parameters and to map the resultant values between [0–1]. The conversion function was as follows:

$$x^* = \frac{x - x_{\min}}{x_{\max} - x_{\min}}, \quad (3)$$

where x^* is the normalized value, x_{\max} is the maximum value, and x_{\min} is the minimum value of the collected data.

The values of MAPE and RMSE are shown in Table 3. Considering the training set with BPNN and GA-BPNN, the MAPE of all the parameters were all below 12%, and the RMSE of these parameters were all at an acceptable level.

However, looking at the test set, the MAPE of penetration (P), cutter torque (T), and advancing thrust (F) were relatively large (10%~15%) with the BPNN model. In this interval, the MAPE and RMSE obtained by the GA-BPNN model were smaller than those obtained by BPNN. More specifically, the MAPE and RMSE of the rotation (R) and penetration (P) were almost the same with those obtained by BPNN, and the fluctuation trend of the two predicted value curves were also consistent. The MAPE and RMSE of rotation (R), advancing thrust (F), and support pressure (W_p) were much smaller, indicating that the GA-BPNN has a better prediction ability for tunnelling parameters, especially for adjustable parameters. The penetration (P) and cutter torque (T) are more likely to be affected by geological and manual operation factors, which could lead to a larger prediction error (but still within the acceptable range).

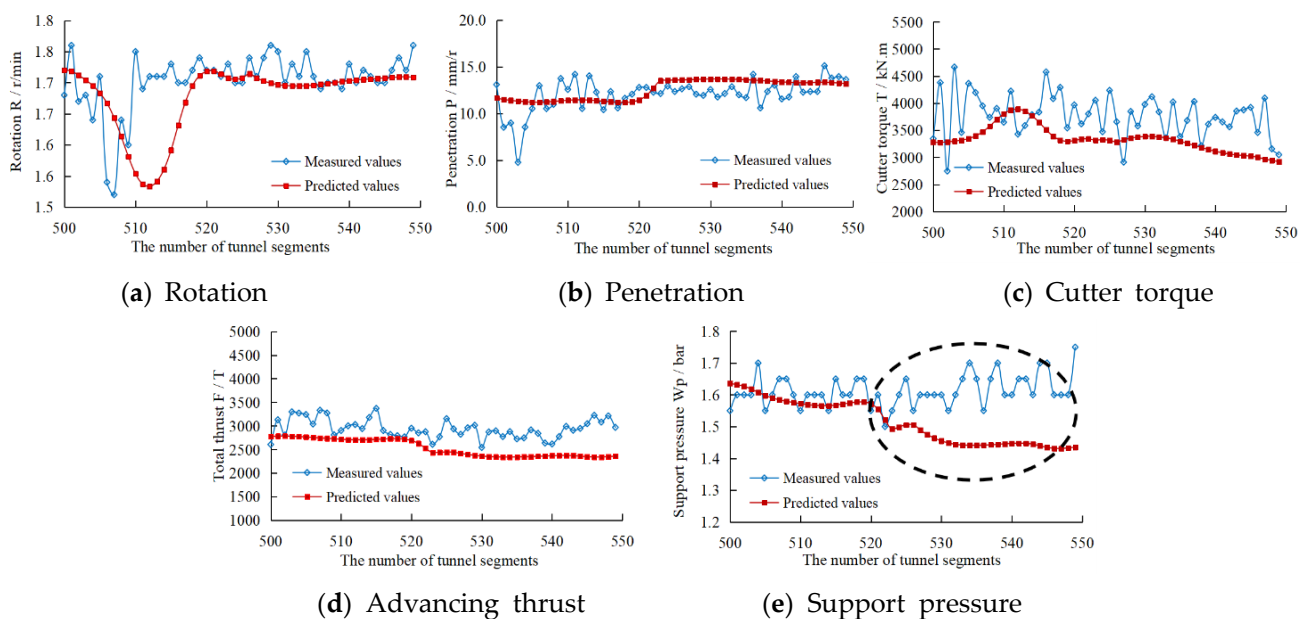


Figure 7. Predicted and measured tunnelling parameters for BPNN: (a) rotation; (b) penetration; (c) cutter torque; (d) advancing thrust; and (e) support pressure.

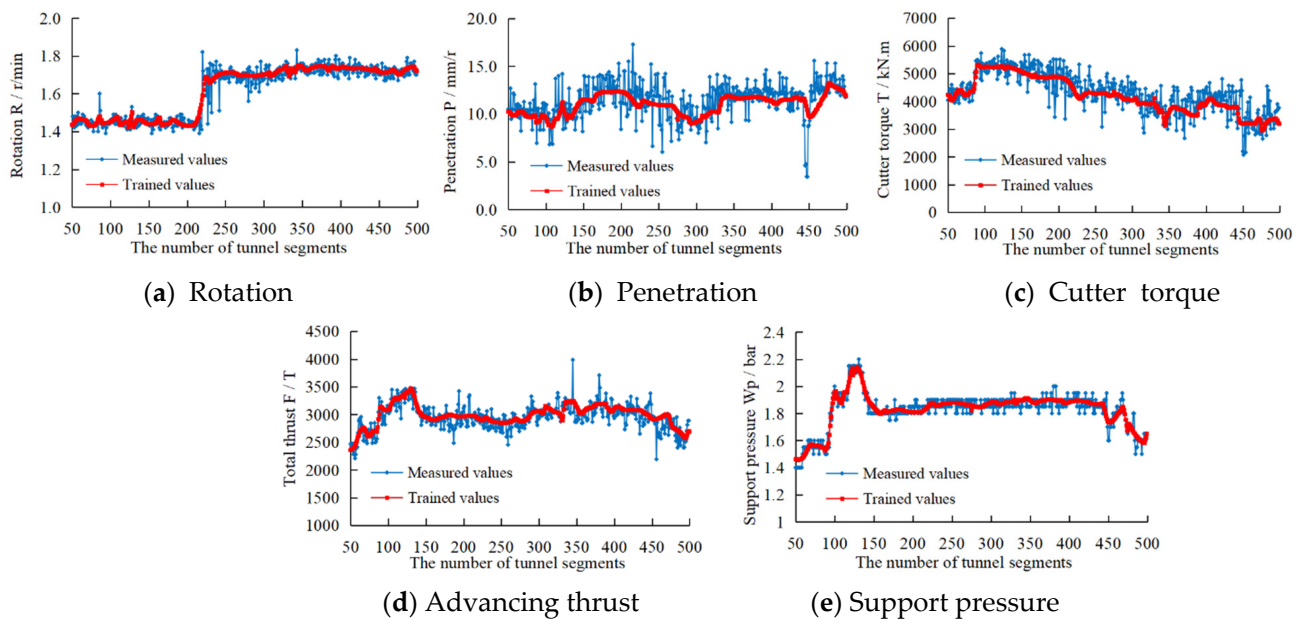


Figure 8. Trained and measured tunnelling parameters for GA-BPNN: (a) rotation; (b) penetration; (c) cutter torque; (d) advancing thrust; and (e) support pressure.

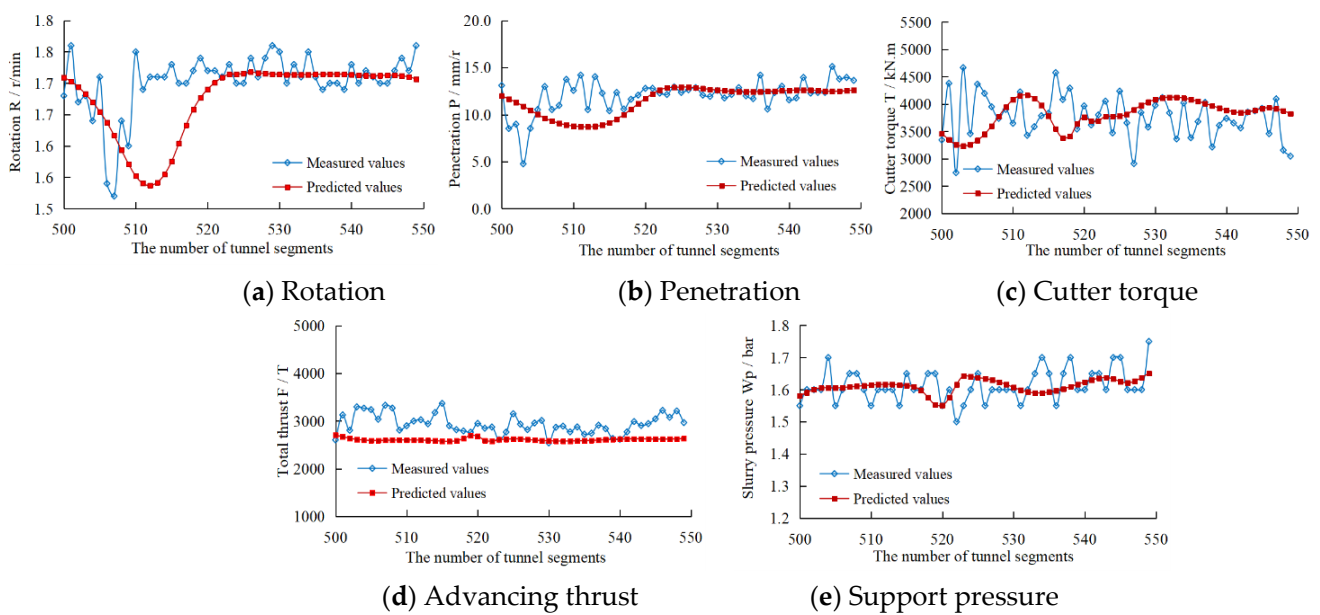


Figure 9. Measured and predicted tunnelling parameters for GA-BPNN: (a) rotation; (b) penetration; (c) cutter torque; (d) advancing thrust; and (e) support pressure.

Table 3. The values of MAPE and RMSE of southern tunnel.

Samples	Index	Rotation/R	Penetration/P	Torque/T	Thrust/F	Pressure/W _p
Training set with BPNN	MAPE	1.7%	11.9%	4.4%	8.5%	2.7%
	RMSE	0.04	1.62	169.42	441.59	0.06
Test set with BPNN	MAPE	2.6%	13.5%	13.9%	13.0%	6.8%
	RMSE	0.07	1.73	464.64	608.88	0.14
Training set with GA-BPNN	MAPE	1.6%	11.6%	4.2%	8.2%	2.0%
	RMSE	0.04	1.61	160.06	421.40	0.05
Test set with GA-BPNN	MAPE	2.7%	14.0%	10.9%	10.5%	2.5%
	RMSE	0.07	2.12	387.28	523.90	0.05

Note that the influencing factors, such as the shield operator's experience and the geological uncertainty, have not been taken into consideration. The predicted curves that were obtained by BPNN and GA-BPNN were smoother than the measured curves. However, the variation trend of the predicted curves is consistent with the measured curves, which were proved by the statistical parameters such as MAPE and RMSE. The training ability of both BPNN and GA-BPNN for tunnelling parameters met the project requirements. However, in terms of the prediction ability and fitting level, GA-BPNN is better than BPNN, especially for adjustable parameters. BPNN may be involved in local optimism, thus reducing its prediction accuracy. However, GA can evaluate multiple solutions in the search space and has a strong global searching ability. Moreover, GA-BPNN showed better performance in capturing the changing trend of the tunnelling parameters.

5. Evaluation of the Ground Reinforcement Effect at the Fine Sand Stratum

5.1. Support Pressure Analysis at Collapse Area of Fine Sand Stratum

Proper support pressure ahead of the shield cutter is one of the most important factors for tunnel stability, especially in the fine sand stratum. If the support pressure is less than the soil pressure in front of the excavation face, it could lead to an unbalanced state between the shield and the stratum, and ground collapse may occur. In order to find the cause of the ground collapse when the north line shield tunneled into the fine sand stratum, the support pressure at the collapse area was analyzed, based on the trained GA-BPNN model, as seen in Figure 10. Compared with the predicted value, the actual support pressure fluctuated greatly, with a higher degree of divergence. When the collapse occurred on the ground surface, the pressure set in this section was only 1.20 bar, which was less than the active limit support pressure (1.30 bar) [32] and the predicted value (1.33 bar). It was observed that when the shield passes through this area, the support pressure should be set at approximately 1.3 bar, and the pressure fluctuation should be controlled within a reasonable range, thus avoiding disturbance to the fine sand stratum.

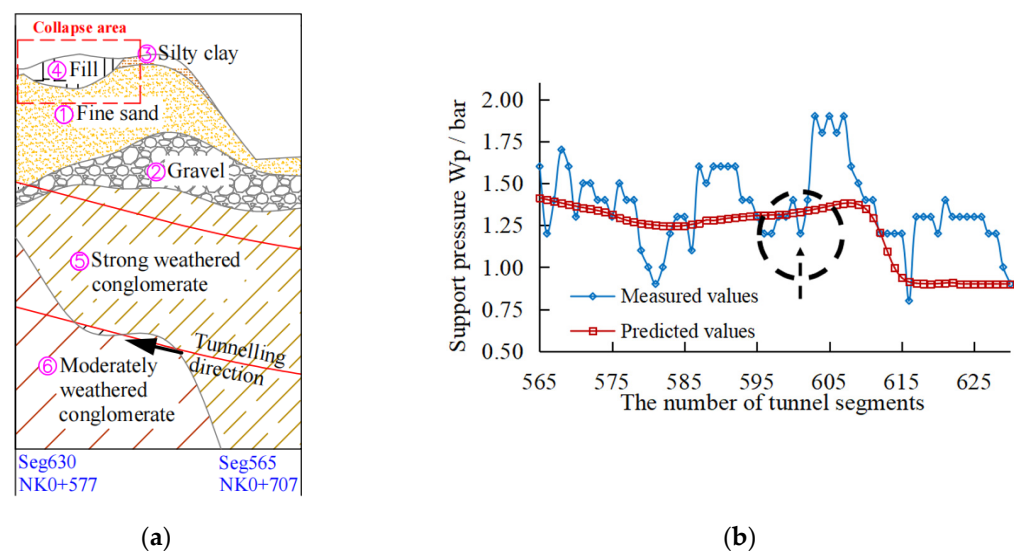


Figure 10. Measured and predicted support pressure at collapse area. (a) Geological conditions at collapse area. (b) Measured and predicted support pressure.

5.2. Tunnelling Parameters Prediction at the Reinforced Stratum

To ensure the safety of the subsequent tunnelling (southern tunnel) in the fine sand stratum and to reduce the risk of ground collapse, the ground grouting reinforcement was adopted before the shield tunnelling into the sand stratum. The longitudinal reinforcement interval was approximately 160 m. The depth of the reinforcement area was from the ground to the strongly weathered conglomerate layer, and the width of it was 6.0 m around

the tunnel. Triple high-pressure $\phi 800$ rotary jet piles were adopted. The reinforcement area is shown in Figure 11.

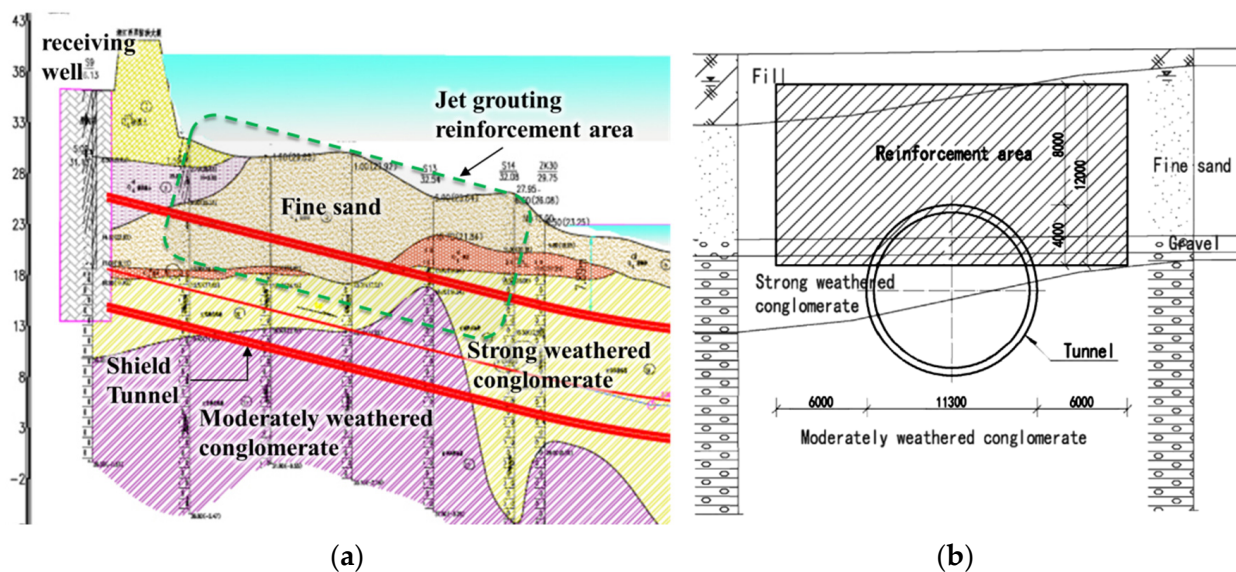


Figure 11. Reinforcement area in the fine sand stratum of southern tunnel. (a) Longitudinal section. (b) Transverse section.

The physical and mechanical parameters of the grout-mixed soil are shown in Table 4. According to previous research [33], the cohesion of the grout-mixed soil is 10–20 times larger than that of the natural soil, and the friction angle is within the range of 20° – 30° .

Table 4. Physical and mechanical properties of the cement–soil.

Stratum	Natural Gravity (kN/m^3)	Cohesion (kPa)	Friction Angle ($^{\circ}$)	Poisson Ratio	Permeability Coefficient (m/d)	Lateral Pressure Coefficient
Mixed cement–soil	20.0	50–100	20–30	0.32	0.01	0.3

Ration (R), advancing thrust (F), and support pressure (W_p) are the three main parameters that can be adjusted during tunnelling, while the penetration (P) and cutter torque (P) are more likely to be affected by geological and other adjustable tunnelling parameters. Before the shield passes through the reinforced area, it is necessary to determine the adjustable tunnelling parameters, reducing the risk of stratum collapse. Based on the trained GA-BPNN model, the tunnelling parameters were predicted, as seen in Figure 12. The upper (cohesion = 100 kPa, friction angle = 30° , and ‘Predicted values U’) and lower (cohesion = 50 kPa, friction angle = 20° , and ‘Predicted values L’) bounds of the shear strength of the grout-mixed soil were considered. The actual tunnelling parameters in the case of reinforcement (southern tunnel, ‘Measured values S’) and non-reinforcement (northern tunnel, ‘Measured values N’) at similar geological sections were also compared.

As seen in Figure 12a, the interval of the predicted rotation with reinforcement (southern tunnel) was 1.66–1.83 r/min. When the shield passed through the grout-reinforced stratum (southern tunnel), the measured rotation was 1.72 r/min, on average. Compared with that at the northern tunnel (0.77 r/min), the value of rotation was increased by nearly 123.3%. The variation of the parameters indicated that the reinforced stratum was relatively homogeneous, thus, the shield could drive smoothly and keep stable, and the tunnelling efficiency was enhanced significantly.

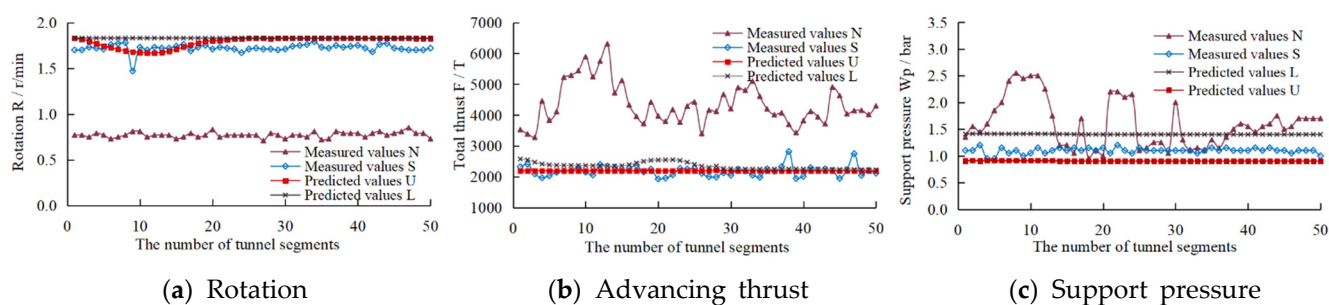


Figure 12. Tunnelling parameters' evaluation: (a) rotation; (b) advancing thrust; and (c) support pressure.

According to previous research [34], 53.5~73% of the energy from a shield's advancing thrust is lost during tunnelling, due to the friction resistance between the shield and stratum. As seen in Figure 12b, the interval of the predicted advancing thrust was 2193–2576 tons. When the shield passed through the reinforced stratum of the southern tunnel, the average advancing thrust was 2190 tons and the standard deviation was 176.70, compared with 4353 tons of average advancing thrust and 667.67 of standard deviation at the northern tunnel. The gaps among them were approximately 98.8% and 277.9%, respectively. When tunnelling through the grout-reinforced stratum, the average advancing thrust was much lower than that of the northern tunnel, with smaller divergence. It indicated that the stratum can maintain stability with smaller advancing thrust after reinforcement, and the energy lost is significantly reduced.

The predicted values of the support pressure obtained by GA-BPNN were fitted with the measured values, as shown in Figure 12c. The interval of the predicted support pressure was 0.90–1.41 bar. When the shield passed through the reinforced stratum of the southern tunnel, the average support pressure was 1.10 bar and the standard deviation was 0.051, compared with 1.60 bar (support pressure) and 0.45 (standard deviation) of that at the northern tunnel—approximately 45.5% and 782.3% lower. It also indicated that the stratum can maintain stability with smaller support pressure after reinforcement.

The predicted tunnelling parameters in grout-reinforced stratum were accurate and were verified by the actual tunnelling parameters. This experience showed that the stability of the pre-reinforced stratum can be ensured, even for cases with a combination of tunnelling parameters at a low-level.

6. Conclusions

In this paper, a neural network model for shield tunnelling parameters was established. In order to improve the stability of the neural network, GA with global searching ability was used to optimize the initial weight of the neural network. Software was developed to implement these functions. This model was applied for the accurate prediction of the tunnelling parameters in an underwater tunnel project in China. The geological conditions, geometric parameters, water depth, and other parameters reflecting the external environmental factors were taken as the input variables, while the tunnelling parameters—such as advancing thrust, rotation, penetration, torque of the cutter head, and support pressure—were taken as the output variables.

As the weight threshold of the BPNN model is randomly assigned, the fitting and prediction accuracy are relatively low. According to the case studies, the prediction errors of penetration, torque, and support pressure are larger than 10%. With the optimization process brought by GA, the prediction accuracy of GA-BPNN was greatly improved, especially for adjustable parameters. The prediction values of tunnelling parameters had a higher coincidence with the measured values, indicating that the GA-BPNN has strong generalization ability, high prediction accuracy, and good consistency.

It is considered that the ground surface collapse was caused by the mismatch between the tunnelling parameters and the formation condition. When a shield passes through

stratum of high risk, the support pressure should be higher than the active limit support pressure, and the pressure fluctuation should be controlled within a reasonable range, avoiding disturbance to the stratum. GA-BPNN can also be used to predict the range of shield tunnelling parameters in stratum of high risk, to guide the setting of operational parameters, and to avoid ground instability.

Shield tunnelling parameters are influenced by many factors, e.g., geological conditions, geometric conditions, and the operator's experience. In this case, two important factors were not taken into account in the GA-BPNN model. The first was the impact of the shield tunnel machine operator's experience, referring to the fact that the shield tunnel machine was working with its nominal, or full capacity. In reality, the shield machine was operated with certain fluctuations. In addition, lack of shield machine experience was also the reason for the prediction bias. This created a difference between the predicted and expected values when estimating the shield performance, especially for the cutter load. The second was the accuracy of the input parameters in the GA-BPNN model. In this paper, the geological parameters at each section were obtained by the linear interpolation method, with the weighted average method. According to every single-borehole geological datum, the possible appearance of rock joints, fractures or mixed ground conditions may be ignored, which brought errors to the prediction of the tunnelling parameters.

Author Contributions: Y.L. identified the research topic and completed the study; K.J. revised and polished a first draft of the paper; S.G. and Y.Y. interpreted the results that were obtained; all co-authors reviewed the paper and agreed to submit the final version of the manuscript to Sustainability. All authors have read and agreed to the published version of the manuscript.

Funding: This research was funded by the Shenzhen Natural Science Foundation (KCXFZ20201221173 207020). The authors are grateful to this institution for their support.

Institutional Review Board Statement: Not applicable.

Informed Consent Statement: Not applicable.

Data Availability Statement: Not applicable.

Conflicts of Interest: The authors declare no conflict of interest.

References

1. Entacher, M.; Lorenz, S.; Galler, R. Tunnel boring machine performance prediction with scaled rock cutting tests. *Int. J. Rock Mech. Min. Sci.* **2014**, *70*, 450–459. [[CrossRef](#)]
2. Rostami, J. Performance prediction of hard rock Tunnel Boring Machines (TBMs) in difficult ground. *Tunn. Undergr. Space Technol.* **2016**, *57*, 173–182. [[CrossRef](#)]
3. Ren, D.J.; Shen, S.L.; Zhou, A.; Chai, J.C. Prediction of lateral continuous wear of cutter ring in soft ground with quartz sand. *Comput. Geotech.* **2018**, *103*, 86–92. [[CrossRef](#)]
4. Zhou, C.; Ding, L.Y.; Zhou, Y.; Skibniewski, M. Visibility graph analysis on time series of shield tunnelling parameters based on complex network theory. *Tunn. Undergr. Space Technol.* **2019**, *89*, 10–24. [[CrossRef](#)]
5. Copur, H.; Aydin, H.; Bilgin, N.; Balci, C.; Tumac, D.; Dayanc, C. Predicting performance of EPB TBMs by using a stochastic model implemented into a deterministic model. *Tunn. Undergr. Space Technol.* **2014**, *42*, 1–14. [[CrossRef](#)]
6. Rostami, J.; Ozdemir, L. A new model for performance production of hard rock TBMs. In Proceedings of the Rapid Excavation and Tunnelling Conferences, Boston, MA, USA, 13–17 June 1993; pp. 793–809. Available online: https://www.researchgate.net/publication/288383954_New_model_for_performance_production_of_hard_rock_TBMs (accessed on 11 October 2022).
7. Rostami, J.; Ozdemir, L.; Nilsen, B. Comparison between CSM and NTH hard rock TBM performance prediction models. In Proceedings of the Annual Technical Meeting of the Institute of Shaft Drilling and Technology, Las Vegas, NV, USA, 1–3 May 1996; pp. 1–11. Available online: https://www.academia.edu/5061945/COMPARISON_BETWEEN_CSM_AND_NTH_HARD_ROCK_TBM_PERFORMANCE_PREDICTION_MODELS_By (accessed on 11 October 2022).
8. Xue, Y.D.; Zhao, F.; Zhao, H.X.; Li, X.; Diao, Z.X. A new method for selecting hard rock TBM tunnelling parameters using optimum energy: A case study. *Tunn. Undergr. Space Technol.* **2018**, *78*, 64–75. [[CrossRef](#)]
9. Bruland, A. Hard Rock Tunnel Boring. Ph.D. Thesis, Norwegian University of Science and Technology, Trondheim, Norway, 1998.
10. Barton, N. *TBM Tunnelling in Jointed and Faulted Rock*; Balkema Brookfield: Rotterdam, The Netherlands, 2000.

11. Bieniawski, Z.T.; Celada, B.; Galera, J.M. TBM excavability: Prediction and machine-rock interaction. In Proceedings of the Rapid Excavation and Tunnelling Conference, Toronto, ON, Canada, 10–13 June 2007; pp. 1118–1130. Available online: https://www.researchgate.net/publication/286943503_TBM_Excavability_Prediction_and_machine-rock_interaction (accessed on 11 October 2022).
12. Delisio, A.; Zhao, J. A new model for TBM performance prediction in blocky rock conditions. *Tunn. Undergr. Space Technol.* **2014**, *43*, 440–452. [[CrossRef](#)]
13. Hassanpour, J.; Rostami, J.; Khamsehchiyan, M.; Bruland, A. Developing new equations for TBM performance prediction in carbonate-argillaceous rocks: A case history of Nowsood water conveyance tunnel. *Geomech. Geoenviron. Int. J.* **2009**, *4*, 287–297. [[CrossRef](#)]
14. Armaghani, D.J.; Mohamad, E.T.; Narayanasamy, M.S.; Narita, N.; Yagiz, S. Development of hybrid intelligent models for predicting TBM penetration rate in hard rock condition. *Tunn. Undergr. Space Technol.* **2017**, *63*, 29–43. [[CrossRef](#)]
15. Benato, A.; Oreste, P. Prediction of penetration per revolution in TBM tunnelling as a function of intact rock and rock mass characteristics. *Int. J. Rock Mech. Min. Sci.* **2015**, *74*, 119–127. [[CrossRef](#)]
16. Salimi, A.; Rostami, J.; Moormann, C.; Delisio, A. Application of non-linear regression analysis and artificial intelligence algorithms for performance prediction of hard rock TBMs. *Tunn. Undergr. Space Technol.* **2016**, *58*, 236–246. [[CrossRef](#)]
17. Mahdevari, S.; Shahriar, K.; Yagiz, S.; Shirazi, M.A. A support vector regression model for predicting tunnel boring machine penetration rates. *Int. J. Rock Mech. Min. Sci.* **2014**, *72*, 214–229. [[CrossRef](#)]
18. Yagiz, S.; Karahan, H. Application of various optimization techniques and comparison of their performances for predicting TBM penetration rate in rock mass. *Int. J. Rock Mech. Min. Sci.* **2015**, *80*, 308–315. [[CrossRef](#)]
19. Ghasemi, E.; Yagiz, S.; Ataei, M. Predicting penetration rate of hard rock tunnel boring machine using fuzzy logic. *Bull. Eng. Geol. Environ.* **2014**, *73*, 23–35. [[CrossRef](#)]
20. Gao, X.J.; Shi, M.L.; Song, X.G.; Zhang, C.; Zhang, H.W. Recurrent neural networks for real-time prediction of TBM operating parameters. *Autom. Constr.* **2019**, *98*, 225–235. [[CrossRef](#)]
21. Sun, W.; Shi, M.L.; Zhang, C.; Zhao, J.H.; Song, X.G. Dynamic load prediction of tunnel boring machine (TBM) based on heterogeneous in-situ data. *Autom. Constr.* **2018**, *92*, 23–34. [[CrossRef](#)]
22. Ye, X.; Wang, S.; Wang, Q.; Sloan, S.W.; Sheng, D. Numerical and experimental studies of the mechanical behaviour for compaction grouted soil nails in sandy soil. *Comput. Geotech.* **2017**, *90*, 202–214. [[CrossRef](#)]
23. Liu, B.; Wang, R.; Zhao, G.; Guo, X.; Wang, Y.; Li, J.; Wang, S. Prediction of rock mass parameters in the TBM tunnel based on BP neural network integrated simulated annealing algorithm. *Tunn. Undergr. Space Technol.* **2020**, *95*, 103103. [[CrossRef](#)]
24. Koopialipour, M.; Fahimifar, A.; Ghaleini, E.N.; Momenzadeh, M.; Armaghani, D.J. Development of a new hybrid ANN for solving a geotechnical problem related to tunnel boring machine performance. *Eng. Comput.* **2020**, *36*, 345–357. [[CrossRef](#)]
25. Wang, S.T.; Wang, J.Z.; Shang, F.K.; Wang, Y.T.; Cheng, Q.; Liu, N. A GA-BP method of detecting carbamate pesticide mixture based on three-dimensional fluorescence spectroscopy. *Spectrochim. Acta Part A Mol. Biomol. Spectrosc.* **2020**, *224*, 117–396. [[CrossRef](#)]
26. Zhang, Q.L.; Liu, Z.Y.; Tan, J.R. Prediction of geological conditions for a tunnel boring machine using big operational data. *Autom. Constr.* **2019**, *100*, 73–83. [[CrossRef](#)]
27. Shi, F.; Wang, X.C.; Yu, L.; Li, Y. *30 Cases of Neural Network Analysis with MATLAB*; Beijing University of Aeronautics and Astronautics Press: Beijing, China, 2010.
28. Lee, H.M.; Chen, C.M.; Huang, T.C. Learning efficiency improvement of back propagation algorithm by error saturation prevention method. *Neurocomputing.* **2001**, *41*, 125–143. [[CrossRef](#)]
29. Liu, X.Y.; Shao, C.; Ma, H.F.; Liu, R.X. Optimal earth pressure balance control for shield tunnelling based on LS-SVM and PSO. *Autom. Constr.* **2011**, *20*, 321–327.
30. Piotrowski, A.P.; Napiorkowski, J. A comparison of methods to avoid overfitting in neural networks training in the case of catchment runoff modelling. *J. Hydrol.* **2013**, *476*, 97–111. [[CrossRef](#)]
31. Liu, X.X. A Research on Population Size Impaction on the Performance of Genetic Algorithm. Master's Thesis, North China Electric Power University (NCEPU), Beijing, China, 2010.
32. Liang, Y.; Chen, X.Y.; Yang, J.S.; Zhang, J.; Huang, L.C. Analysis of ground collapse caused by shield tunnelling and the evaluation of the reinforcement effect on a sand stratum. *Eng. Fail. Anal.* **2020**, *115*, 104–616. [[CrossRef](#)]
33. Pinto, F.; Zymnis, D.M. Ground movements due to shallow tunnels in soft ground. II: Analytical interpretation and prediction. *J. Geotech. Geoenviron. Eng.* **2014**, *140*, 80–90. [[CrossRef](#)]
34. Xu, Q.W.; Zhu, H.H.; Ding, W.Q.; Wu, X.S.; Yu, N. Cutting torque during tunnelling process of earth pressure balance shield machine in homogeneous ground. *Chin. J. Geotech. Eng.* **2010**, *32*, 47–54.